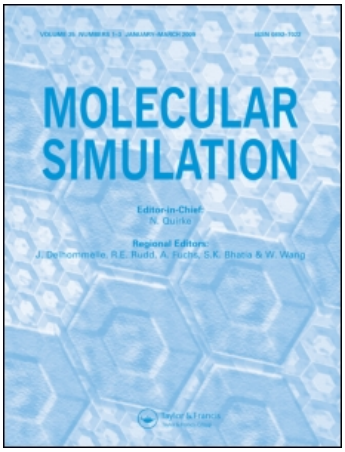

Molecular Simulation
Publication details, including instructions for authors and subscription information:
http://www.informaworld.com/smpp/title~content=t713644482

Shear viscosity and thermal conductivity of quadrupolar real fluids from molecular simulation

G. A. Fernández[a]; J. Vrabec[a]; H. Hasse[a]
[a] Institute of Thermodynamics and Thermal Process Engineering, University of Stuttgart, Stuttgart, Germany

To cite this Article Fernández, G. A. , Vrabec, J. and Hasse, H.(2005) 'Shear viscosity and thermal conductivity of quadrupolar real fluids from molecular simulation', Molecular Simulation, 31: 11, 787 — 793
To link to this Article: DOI: 10.1080/08927020500252599
URL: http://dx.doi.org/10.1080/08927020500252599

Molecular Simulation, Vol. 31, No. 11, 15 September 2005, 787–793

Taylor & Francis
Taylor & Francis Group

Shear viscosity and thermal conductivity of quadrupolar real fluids from molecular simulation

G. A. FERNÁNDEZ, J. VRABEC* and H. HASSE

Institute of Thermodynamics and Thermal Process Engineering, University of Stuttgart, D-70550 Stuttgart, Germany

(Received April 2005; in final form April 2005)

In the present work, equilibrium molecular dynamics was used with the Green-Kubo formalism to simultaneously calculate shear viscosity and thermal conductivity of ten real fluids, i.e. F_2, N_2, O_2, CO_2, C_2H_6, C_2H_4, C_2F_6, C_3H_4, C_3H_6 and SF_6. The fluids were consistently described by the two-center Lennard–Jones plus point quadrupole (2CLJQ) pair potential, whose parameters were adjusted to vapor–liquid equilibria only [J. Phys. Chem. B, 2001, 105, 12126–12133]. The predicted shear viscosities and thermal conductivities show an overall average deviation of only about 10% from correlations of experimental data where comparison was possible.

At low temperature and high density state points, the Green–Kubo integral for shear viscosity shows slow convergence. This problem can be overcome by a new approach developed in the present work. It is based on the adjustment of a suitable function describing the long time behavior of the autocorrelation function and yields reliable results without the need of excessively long simulation runs.

Keywords: Shear viscosity; Thermal conductivity; Green–Kubo; Molecular simulation

1. Introduction

Transport properties are important in many technical and natural processes. Usually, transport properties are obtained by measurement or estimated using empirical correlations. However, for many systems no experimental data are available or the empirical correlations are not adequate. In the last decades, with the increasing computing power, molecular simulation in combination with molecular modeling is becoming an interesting option for obtaining transport properties, especially when they are needed under extreme conditions [1]. Currently, there exist two standard methodologies to obtain transport coefficients from molecular simulation, i.e. non-equilibrium molecular dynamics (NEMD) and equilibrium molecular dynamics (EMD). In NEMD, transport coefficients are calculated as the ratio of a flux to an appropriate driving force, extrapolating to the limit of zero driving force [2–4]. In EMD, transport coefficients are in most cases calculated by the Green–Kubo formalism [6,7]. The choice between EMD and NEMD is largely a matter of taste and inclination, see e.g. [8–10]. In the present work, the Green–Kubo method is preferred over NEMD, due to the fact that it allows to calculate several transport coefficients in one simulation run.

In recent works, we investigated the performance of molecular models, which were adjusted to vapor–liquid equilibria only, to predict transport properties of noble gases and methane. For these simple fluids and their mixtures, good predictions of self and Maxwell–Stefan diffusion coefficients, shear and bulk viscosities as well as thermal conductivities were found [11,12]. This investigation has now been extended to more complex molecules considering anisotropy and quadrupolarity. These models have already been successfully tested in the prediction of self-diffusion coefficients [13]. In the present work predictions of shear viscosity and thermal conductivity, based on the 2CLJQ potential are assessed for F_2, N_2, O_2, CO_2, C_2H_6, C_2H_4, C_2F_6, C_3H_4, C_3H_6 and SF_6.

The 2CLJQ model has successfully been employed by several authors, for the description of thermodynamic properties [14–17], Joule–Thomson inversion curves [18] and self-diffusion coefficients [13]. Albeit the 2CLJQ potential is not new, the prediction of transport properties with the 2CLJQ model, has up to now not been explored in detail. In order to overcome this, shear viscosity and thermal conductivity were determined in the present work and compared to accurate correlations of experimental data, where this was possible.

Early works [19] showed that the autocorrelation function for shear viscosity exhibits a long time behavior close to the phase boundary to solidification giving raise to a slow convergence of the Green–Kubo integral. Taking

*Corresponding author. Tel.: +49-711/685-6107. Fax: +49-711/685-6140. E-mail: vrabec@itt.uni-stuttgart.de

Molecular Simulation
ISSN 0892-7022 print/ISSN 1029-0435 online © 2005 Taylor & Francis
http://www.tandf.co.uk/journals
DOI: 10.1080/08927020500252599

into account the good performance of those models at other state points, the convergence of the Green–Kubo integrals for thermal conductivity and shear viscosity is investigated for F_2 at the highest density state points. Subsequently, an approach to address this problem with low computational cost is introduced.

2. Method

2.1 Molecular models

The intermolecular interactions are represented by the two-center Lennard–Jones plus point quadrupole (2CLJQ) potential. The 2CLJQ model is a pairwise additive potential consisting of two Lennard–Jones (LJ) sites, a distance L apart plus a point quadrupole of momentum Q placed in the geometric center of the molecule oriented along the molecular axis connecting the two LJ sites. The interaction energy of two molecules i and j is

$$u_{ij}^{2CLJQ} = \sum_{a=1}^{2}\sum_{b=1}^{2} 4\epsilon\left[\left(\frac{\sigma}{r_{ab}}\right)^{12} - \left(\frac{\sigma}{r_{ab}}\right)^{6}\right] + u_Q. \quad (1)$$

Here, r_{ab} is one of the four LJ site–site distances; a counts the two LJ sites of molecule i, b counts those of molecule j. The LJ parameters σ and ϵ represent size and energy, respectively. The contribution of a point quadrupole is given by [20]

$$u_Q = \frac{3}{4}\frac{Q^2}{|\mathbf{r}_{ij}|^5}[1-5(c_i^2+c_j^2)-15c_i^2c_j^2+2(s_is_jc-4c_ic_j)^2], \quad (2)$$

with $c_k = \cos\theta_k$, $s_k = \sin\theta_k$ and $c = \cos\phi_{ij}$. Herein $\mathbf{r}_{ij}$ is the center–center distance vector of two molecules i and j. θ_i is the angle between the axis of the molecule i and the center–center connection line and ϕ_{ij} is the azimutal angle between the axis of molecules i and j. Equation (2) has only one adjustable parameter, namely the quadrupolar momentum Q.

Pure substance parameters σ, ϵ, L and Q were taken from Vrabec *et al.* [17] as given in table 1. They were adjusted in [17] exclusively to experimental pure substance vapor–liquid equilibrium data. For symmetric diatomic molecules (F_2, N_2, O_2) and symmetric triatomic molecules (CO_2), as well as C_2 and C_3 derivatives (C_2H_6, C_2H_4, C_2F_6, C_3H_4, C_3H_6) modeling with the 2CLJQ potential represents a good approximation. As a test case, SF_6 was also modeled by the 2CLJQ potential [17] but the fitted elongation and quadrupolar momentum lose all physical meaning.

Table 1. Potential model parameters for the pure fluids used in this work.[a,b]

Fluid	σ/(Å)	ϵ/k_B/(K)	L/(Å)	Q/(DÅ)	M/(g mol^{-1})
F_2	2.8258	52.147	1.4129	0.8920	38.00
N_2	3.3211	34.897	1.0464	1.4397	28.01
O_2	3.1062	43.183	0.9699	0.8081	32.00
CO_2	2.9847	133.22	2.4176	3.7938	44.01
C_2H_6	3.4896	136.99	2.3762	0.8277	30.07
C_2H_4	3.7607	76.950	1.2695	4.3310	28.05
C_2F_6	4.1282	110.19	2.7246	8.4943	138.01
C_3H_6	3.8169	150.78	2.5014	5.9387	48.08
C_3H_4	3.5460	186.43	2.8368	5.7548	40.06
SF_6	3.9615	118.98	2.6375	8.0066	146.06

[a] Values taken from [15]. [b] The molar mass M was taken from [33].

2.2 Shear viscosity and thermal conductivity

The shear viscosity η, as defined in Newton's "law" of viscosity, describes the resistance of a fluid to shear forces. It refers to the resistance of an infinitesimal volume element to shear at constant volume [21]. The shear viscosity can also be related to momentum transport under the influence of velocity gradients. From a microscopic point of view, the shear viscosity can be calculated by integration of the time-autocorrelation function of the off diagonal elements of the stress tensor, i.e. J_p^{xy} [22,23]

$$\eta = \frac{1}{Vk_BT}\int_0^\infty \mathrm{d}t\langle J_p^{xy}(t)\cdot J_p^{xy}(0)\rangle, \quad (3)$$

where V is the molar volume, k_B is the Boltzmann constant, T the temperature and $<\ldots>$ denotes the ensemble average. The statistics of the ensemble average in equation (3) can be improved using all three independent off diagonal elements of the stress tensor, i.e. J_p^{xy}, J_p^{xz} and J_p^{yz}. For a pure fluid, the component J_p^{xy} of the microscopic stress tensor $\mathbf{J}_p$ is given by [24]

$$J_p^{xy} = \sum_{i=1}^{N} m_i v_i^x v_i^y - \frac{1}{2}\sum_{i=1}^{N}\sum_{j\neq i}^{N}\sum_{k=1}^{3}\sum_{l=1}^{3} r_{ij}^x \frac{\partial u_{ij}}{\partial r_{kl}^y}. \quad (4)$$

Here, i and j are the molecular indices. Subindices l and k count all sites, including the quadrupolar site, and the upper indices x and y denote the vector component, e.g. for velocity v_i^x or center–center distance r_{ij}^x. The mass of molecule i is represented by m_i.

2.3 Thermal conductivity

The thermal conductivity λ, as defined in Fourier's "law" of heat conduction, characterizes the capability of a substance for molecular transport of energy driven by temperature gradients. It can be calculated by integration of the time-autocorrelation function of the elements of the microscopic heat flow J_q^x, and is given by [22,23]

$$\lambda = \frac{1}{Vk_BT^2}\int_0^\infty \mathrm{d}t\langle J_q^x(t)\cdot J_q^x(0)\rangle. \quad (5)$$

The expression for the heat flow $\mathbf{J}_q$ in pure fluids have been derived by Evans [24] and is given by

$$\mathbf{J}_\mathrm{q} = \frac{1}{2}\sum_{i=1}^{N}\left(\left(m_iv_i^2 + \mathbf{w}_\mathrm{i}\mathbf{I}_\mathrm{i}\mathbf{w}_\mathrm{i} + \sum_{j\neq 1}^{N} u_{ij}\right)\cdot \mathbf{v}_i\right) - \frac{1}{2}\sum_{i=1}^{N}\sum_{j\neq i}^{N}\sum_{k=1}^{3}\sum_{l=1}^{3}\mathbf{r}_\mathrm{ij}\cdot\left(\mathbf{v}_i\frac{\partial \mathrm{u}_\mathrm{ij}}{\partial \mathbf{r}_\mathrm{kl}} + \mathbf{w}_\mathrm{i}\Gamma_\mathrm{ij}\right), \quad (6)$$

where $\mathbf{w}_i$ is the angular velocity vector of molecule i, $\mathbf{I}_i$ the matrix of angular momentum of inertia, u_{ij} the intermolecular potential energy and $\boldsymbol{\Gamma}_{ij}$ is the torque. The

torque refers to a reference frame with origin in the molecular center of mass.

2.4 Simulation details

Equilibrium molecular dynamics simulations were performed in a cubic box of volume V containing $N = 500$ molecules. The cut-off radius was set to $r_c = 5\sigma$ and the molecules in the fluid were assumed to have no preferential relative orientations outside of the cut-off sphere. For the calculation of the LJ long-range corrections, orientational averaging was done with equally weighted relative orientations as proposed by Lustig [25]. The assumption of no preferential relative orientations beyond the cut-off sphere, implies that no long-range corrections for the quadrupolar interactions are needed since they disappear. The simulations were started with the molecules in a face centered cubic lattice with random velocities, the total momentum of the system was set to zero, and Newton's equations of motion were solved with the Gear predictor–corrector integration scheme of fifth order [26]. The time step for this algorithm was set to $\Delta t \cdot \sqrt{\epsilon/m}/\sigma = 0.0005$. The shear viscosity and thermal conductivity were calculated in the microcanonical *NVE* ensemble using equations (3)–(6). The simulations were equilibrated in the canonical *NVT* ensemble between 100,000 and 150,000 time steps. Once the equilibrium in the *NVT* ensemble is reached, the *NVT* thermostat was turned off and the simulation continued in the *NVE* ensemble where the shear viscosity and thermal conductivity were calculated. The temperature drift was less than 3% in the worst case. The statistical uncertainty was estimated using Fincham's method [28] averaging over 6000 independent autocorrelation functions in most cases, otherwise two independent simulations were carried out at the same state point, calculating 3000 independent autocorrelations functions in each. In this case, the statistical uncertainty was estimated with the standard deviations of the two simulations. In this work, between 600,000 and 1,800,000 time steps were performed in each simulation.

3. Results

In this section the predictions for shear viscosity and thermal conductivity are compared to correlations of experimental data. In all cases the studied state points correspond to the saturated liquid. The densities as well as the reference to compare viscosities and thermal conductivities were taken from the REFPROP program of Lemmon *et al.* [29] provided by NIST. In this program, all correlations for density are based on experimental data and are accurate; deviations vary from 0.05% for CO_2 to 0.6% for N_2. On the other hand, for the viscosities and thermal conductivities there exist two categories of correlations. The correlations for N_2, O_2, CO_2, C_2H_2, C_2H_4, C_2F_6 and C_3H_6 are in the first category; they are entirely based on experimental data and show deviations from the experiment that vary from 2% for N_2 up to 10% in the case of C_2H_4. Although they fit the experimental data within a few percent, the correlation for C_2F_6 could be less reliable than the others because it was fitted over a limited number of data points. The correlations for F_2, C_3H_4 and SF_6 are in the second category, where no experimental data were available and an extended principle of corresponding states in a predictive form was used. These values correspond to information contained in the REFPROP program and it only refers to the liquid state. It must be pointed out that those correlations of experimental data are more accurate than isolated experimental data, because the experimental scatter tends to be compensated in correlations. That is the main reason why they were preferred here in place of primary experimental data. Furthermore, additional experimental data of shear viscosity for F_2 [30] are included in the comparison. For reasons of clarity, the fluids were grouped in figures 1–4 according to their density, from low to high.

3.1 Shear viscosity

Figure 1 shows the results for the shear viscosity of C_2F_6, SF_6, C_3H_6, C_3H_4 and C_2H_6. Overall, very good agreement between experiment and simulation is found. With the exception of C_2F_6, almost all results agree within their statistical uncertainties with the correlations. The best results are obtained for C_3H_6 for which the average deviation is only 4%, for C_3H_4, SF_6 and C_2H_6 the average deviations are lower than 10%. The poorest results are found for C_2F_6 being systematically too low with an average deviation of 27%.

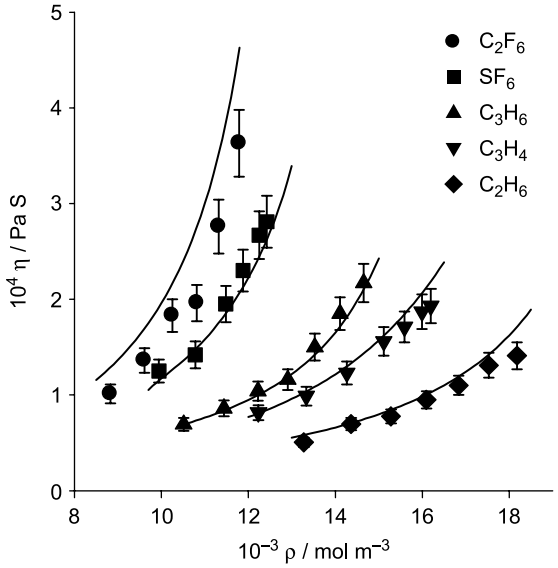

Figure 1. Shear viscosity of saturated liquids. The simulations are shown at regular intervals of $0.05T_c$, where T_c is the critical temperature of the fluid. Simulation results: C_2F_6 ($T = 190.5$–263.7 K): •, SF_6 ($T = 230.0$–286.8 K): ■, C_3H_6 ($T = 219.3$–329.0 K): ▲, C_3H_4 ($T = 275.0$–362.1 K): ▼, C_2H_6 ($T = 182.5$–273.7 K): ◆. Solid lines represent the results of REFPROP [29].

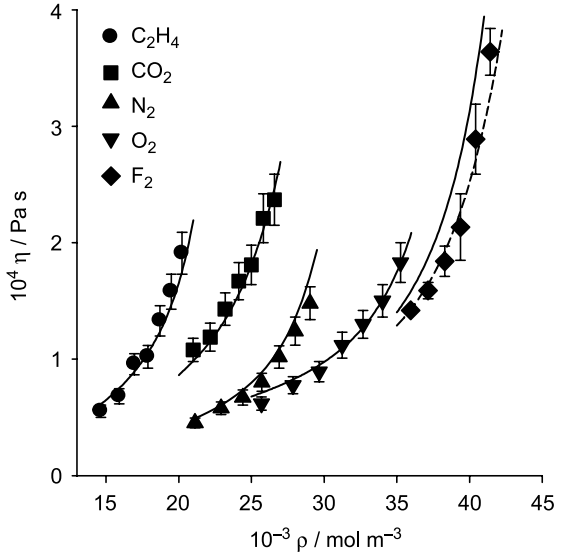

Figure 2. Shear viscosity of saturated liquids. The simulations are shown at regular intervals of $0.05T_c$. Simulation results: C_2H_4 ($T = 169.4$–254.1 K): •, CO_2 ($T = 218.9$–273.7 K): ■, N_2 ($T = 75.7$–113.5 K): ▲, O_2 ($T = 92.7$–139.1 K): ▼, F_2 ($T = 74.4$–102.9 K): ◆. The values for F_2 include the correction due to the long time tail. Solid lines represent the results of REFPROP [29], and the dashed line represents experimental data for F_2 [30].

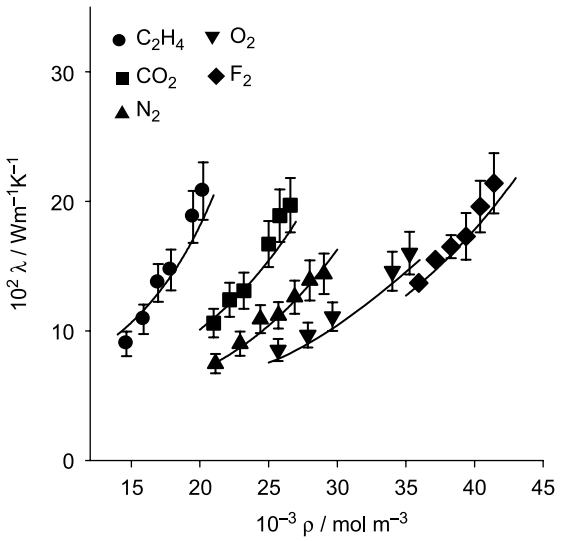

Figure 4. Thermal conductivity of saturated liquids. The simulations are shown at regular intervals of $0.05T_c$. Simulation results: C_2H_4 ($T = 169.4$–254.1 K): •, CO_2 ($T = 218.9$–237.2, 255.5–273.7 K): ■, N_2 ($T = 75.7$–113.5 K): ▲, O_2 ($T = 92.7$–100.5, 123.7–139.1 K): ▼, F_2 ($T = 74.4$–102.9 K): ◆. Solid lines represent the results of REFPROP [29].

Figure 2 shows the results for the shear viscosity of C_2H_4, CO_2, N_2, O_2 and F_2. As for the fluids discussed above the agreement between experiment and simulation is within their uncertainties, with the exception of F_2. The best results are obtained for O_2 and CO_2 for which the average deviations are only 4 and 5%, respectively, whereas for N_2 and C_2H_4 average deviations of up to 10% occur. On the other hand, for F_2, a fluid for which thermal and caloric properties are well described by the 2CLJQ model [17], systematic deviations from the predictive correlation, with an average of 16%, are observed. On the other hand, the agreement of the simulations with the experimental data [30], c.f. dash line in figure 2, is practically within the simulation uncertainties, with an average deviation of 5%. Here the simulations are clearly more accurate than the predictive model, demonstrating the predictive power of the molecular models.

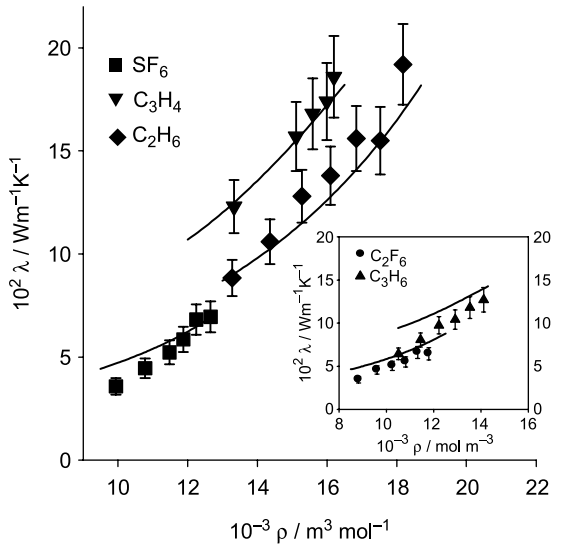

Figure 3. Shear viscosity of saturated liquids. The simulations are shown at regular intervals of $0.05T_c$. Simulation results: C_2F_6 ($T = 190.5$–263.7 K): •, SF_6 ($T = 223.0$, 235.0–286.8 K): ■, C_3H_6 ($T = 237.6$–329.0 K): ▲, C_3H_4 ($T = 275.0$–301.8, 342.0 K): ▼, C_2H_6 ($T = 182.5$–273.7 K): ◆. Solid lines represent the results of REFPROP [29].

3.2 Thermal conductivity

Figure 3 shows the results for the thermal conductivity of C_2H_6, C_2F_6, C_3H_4, C_3H_6 and SF_6. Overall, good agreement between experiment and simulation is found. For C_3H_6, C_3H_4 and SF_6 almost all simulation results agree within their statistical uncertainties, for C_3H_6 and C_2F_6 the simulations are too low by about 20%.

In figure 4 the results for the thermal conductivity of F_2, N_2, O_2, CO_2 and C_2H_4 are presented. Overall, very good agreement between the correlations of experimental data and the simulations is found, the deviations are throughout within the simulation uncertainty. For these five fluids the average deviations between the simulations and the correlations of experimental data are lower than 10%.

Figure 5 summarizes the results in a bar chart. With the exception of C_2F_6 for shear viscosity, as well as C_2F_6 and C_3H_6 for thermal conductivity, deviations being lower than 10% from the correlations are observed. These two fluids present deviations, which are about two times larger than the average. Moreover, C_2F_6 shows the largest deviations for both shear viscosity and thermal conductivity. These larger differences could reside more in the limited data set used in the correlation for C_2F_6 than in the performance of the

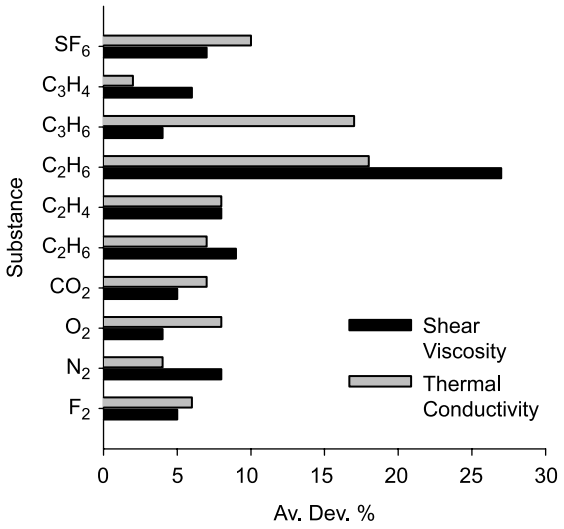

Figure 5. Average deviations of shear viscosity and thermal conductivity of saturated liquid F_2, N_2, O_2, CO_2, C_2H_6, C_2H_4, C_2F_6, C_3H_4, C_3H_6 and SF_6 from REFPROP [29].

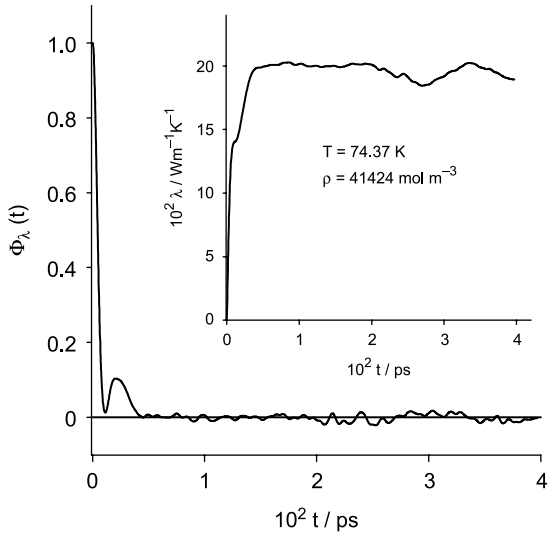

Figure 6. Large plot: autocorrelation function of thermal conductivity. Small plot: integral of the autocorrelation function for the thermal conductivity. Both plots are for the most dense simulated state point of saturated liquid fluorine.

molecular model used for this fluid. If these two fluids are not considered at all, the average deviations are lower than 7%, that is lower than the simulations uncertainty. In general, the deviations for viscosity are slightly larger than for thermal conductivity.

3.3 Long time behavior of the Green–Kubo Integrals

Early simulations of hard spheres of Alder *et al.* [19] suggest the existence of a long time tail in the autocorrelation function of viscosity near the phase boundary to solidification due to the low compressibility of the liquid. This behavior was also found in spherical LJ fluid simulations by Levesque *et al.* [31] and later by Schoen and Hoheisel [32]. This causes problems in the convergence of the Green–Kubo integral, since the correlation function must be calculated over a longer time span. As the F_2 state points correspond to the highest density among the studied fluids, the convergence of the Green–Kubo integrals is investigated for this substance.

Figure 6 shows the calculated autocorrelation function of thermal conductivity and its integral, cf. equation (5), at the state point $T = 74.4\,\mathrm{K}$ and $\rho = 41424\,\mathrm{mol\,m^{-3}}$. These conditions correspond to 92% of the triple point density (triple point temperature is $T = 53.4\,\mathrm{K}$). The time correlation function exhibits a fast decay during the first $0.1 \times 10^{-2}\,\mathrm{ps}$, afterwards its rises to decay again very fast. The small plot in figure 6 shows that the Green–Kubo integral converges approximately after $10^{-2}\,\mathrm{ps}$ within the uncertainty of the simulation. No significant contribution to the integral after $10^{-2}\,\mathrm{ps}$ was observed.

The autocorrelation function of shear viscosity is plotted in figure 7 for the same state point. It does exhibit a long time tail. Its influence on the shear viscosity can be seen better in the small plot in figure 7, where the integrals for the six saturated liquid densities between $T = 74.4$ and $102.9\,\mathrm{K}$ are shown. The corresponding thermodynamic conditions are given in table 2. The simulations for state points 4–6 converge approximately after $1.5 \times 10^{-2}\,\mathrm{ps}$, that for state point 3 after $2 \times 10^{-2}\,\mathrm{ps}$. For state point 2, convergence is reached only after about $3 \times 10^{-2}\,\mathrm{ps}$, whereas for state point 1 it is questionable if convergence is reached at all in the simulation run of about $4 \times 10^{-2}\,\mathrm{ps}$. In order to overcome this problem with reasonable computational effort, the autocorrelation function of the shear viscosity $\phi(t) = J_p^{xy}(0) \cdot J_p^{xy}(t)/(J_p^{xy}(0) \cdot J_p^{xy}(0))$ was assumed to decay exponentially for times larger than $1.5 \times 10^{-2}\,\mathrm{ps}$. Therefore, for $1.5\text{–}4 \times 10^{-2}\,\mathrm{ps}$ an exponential function of the form $\phi^{\mathrm{fit}}(t) = a\exp(-t/b)$ was fitted to the simulation data and extrapolated to infinity.

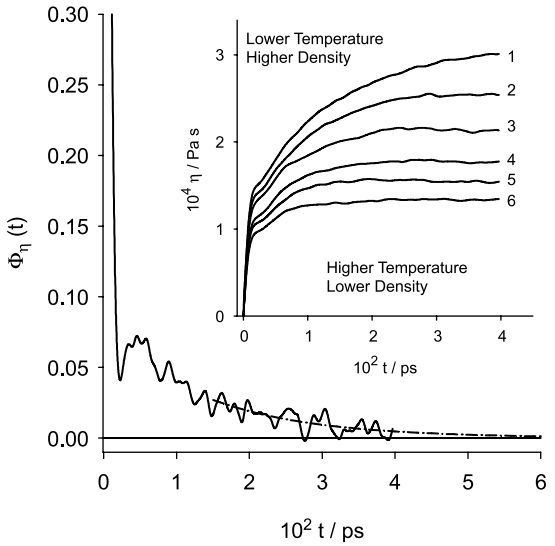

Figure 7. Large plot: autocorrelation function of the shear viscosity —. Fitted function _.._.. Small plot: integrals for all six simulated state points of saturated liquid fluorine, numbers 1–6 refer to table 2.

Table 2. Shear viscosity η for F_2 calculated by molecular dynamics without long time tail.

State point no.	T (K)	ρ (mol m^{-3})	η (10^4 Pa s)	Δη (10^4 Pa s)
1	74.4	41424	3.01 (20)	0.63
2	80.1	40422	2.54 (30)	0.35
3	85.8	39382	2.13 (30)	
4	91.2	38295	1.84 (13)	
5	97.3	37153	1.59 (7)	
6	103.0	35946	1.42 (3)	

The correction due to the long time tail is denoted by $\Delta\eta$, calculated by integration of the fitted function. The numbers in parentheses denote the uncertainty in the last digits.

The choice of an exponential function can be justified by comparison with the Enskog theory [19,34].

In this way, the shear viscosity for state points 1 and 2 was estimated as the integral over the autocorrelation function of shear viscosity $\phi(t)$, where it is composed of the explicitly simulated part and the fitted exponential function, i.e. $\phi(t) = \phi^{\text{sim}}(t) + \phi^{\text{fit}}(t)$. In table 2, the estimated values of the shear viscosity for the state points 1 and 2, together with the contributions of the corrections due to the long time behavior, $\Delta\eta$, are given. The contributions of the long time tail is about 20 and 10% for state points 1 and 2, respectively. These contributions are in the order of magnitude of the statistical uncertainty of the simulations. However, they improve significantly the results indicating clearly that the contribution of the long time tail must be considered for state points close to solidification. Otherwise, a longer calculation of the autocorrelation function is necessary. However, taking into account the inherent simulation uncertainties, which makes difficult to find the point where the correlation function does not contribute any more to the integral, the procedure adopted here is straightforward and much more economic in terms of computation time.

4. Conclusion

In the present work, the Green–Kubo formalism was used to calculate simultaneously shear viscosity and thermal conductivity for ten fluids, i.e. F_2, N_2, O_2, CO_2, C_2H_6, C_2H_4, C_2F_6, C_3H_4, C_3H_6 and SF_6 along the bubble line. The molecular interactions of the fluids were modeled with the 2CLJQ potential with parameters adjusted to vapor–liquid equilibria only. The comparison with available correlations of experimental data shows good agreement. This agreement is especially remarkable in the case of thermal conductivity since internal degrees of freedom were not taken into account in the simple models used here.

The present results, together with those of previous studies [13,17] show that static thermodynamic properties [17,18] and transport properties like self-diffusion coefficients [13], viscosity and thermal conductivity can simultaneously be described for the studied fluids with simple molecular models.

The convergence of the Green–Kubo integrals of thermal conductivity and shear viscosity for state points close to the solid–liquid phase boundary were investigated. The Green–Kubo integral for thermal conductivity converges to its final value quickly (after 10^{-2} ps). On the other hand, the Green–Kubo integral for shear viscosity shows a slow convergence for state points close to the solid–liquid phase boundary. An approach to overcome this problem is presented. It consists of the extrapolation of the autocorrelation functions for long times with a suitable function; in this case, an exponential function was selected. It allows to correct the truncation error of the Green–Kubo integral with low computational cost. This correction contributes up to 20% in the shear viscosity for the most dense state point studied here.

Recent results indicate that better agreement can be obtained if transport properties are used directly in the parameterization of the molecular potential [33]. On the other hand, the parameterization to vapor–liquid equilibria allows not only the prediction of some static properties but also transport properties with good accuracy. Finally, the successful prediction of transport properties with simple models as those used here is remarkable and encouraging for molecular modeling.

References

[1] C. McCabe, S. Cui, P.T. Cummings, P.A. Gordon, R.B. Saeger. Examing the rheology of 9-octylheptadecane to giga-pascal pressure. *J. Chem. Phys.*, **114**, 1887 (2001).

[2] D.J. Evans, G.P. Morris. *Statistical Mechanics of Nonequilibrium Liquids*, Academic Press, London (1990), Chapter 6.

[3] S.S. Sarman, D.J. Evans, P.T. Cummings. Recent developments in non-Newtonian molecular dynamics. *Phys. Rep.*, **305**, 1 (1998).

[4] B.D. Tood. Computer simulation of simple and complex atomistic fluids by nonequilibrium molecular dynamics techniques. *Comp. Phys. Commun.*, **142**, 14 (2001).

[5] B.J. Alder, T.E. Wainwright. Decay of the velocity autocorrelation function. *Phys. Rev. A*, **1**, 18 (1967).

[6] M.S. Green. Markoff random processes and the statistical mechanics of the time–dependent phenomena II. Irreversible processes in fluids. *J. Chem. Phys.*, **22**, 398 (1954).

[7] R. Kubo. Statistical–mechanical theory of irreversible processes I. *J. Phys. Soc. Jpn*, **12**, 570 (1957).

[8] B.L. Holian, D.J. Evans. Shear viscosity away from the melting line: A comparison of equilibrium and nonequilibrium molecular dynamics. *J. Chem. Phys.*, **78**, 5147 (1983).

[9] J.J. Erpenbeck. Comparison of Green–Kubo and nonequilibrium calculations of the self-diffusion constant of a Lennard–Jones fluid. *Phys. Rev. A*, **35**, 218 (1987).

[10] S.T. Cui, P.T. Cummings, H.D. Cochran. The calculation of viscosity of liquid n-decane and n-hexadecane by the Green–Kubo methods. *Mol. Phys.*, **93**, 117 (1998).

[11] G.A. Fernández, J. Vrabec, H. Hasse. Self diffusion and binary Maxwell–Stefan diffusion in simple fluids with the Green–Kubo method. *Int. J. Thermophys.*, **25**, 175 (2004).

[12] G.A. Fernández, J. Vrabec, H. Hasse. A molecular simulation study of shear and bulk viscosity and thermal conductivity of simple real fluids. *Fluid Phase Equilibria*, **221**, 157 (2004).

[13] G.A. Fernández, J. Vrabec, H. Hasse. Self-diffusion and binary Maxwell–Stefan diffusion coefficients of quadrupolar real fluids from molecular simulation. *Int. J. Thermophys.*, (2005), accepted.

[14] P.S.Y. Cheung, J.G. Powles. The properties of liquid nitrogen IV. A computer simulation. *Mol. Phys.*, **30**, 921 (1975).

[15] R. Vogelsang, C. Hoheisel. Comparison of various potential models for the simulation of pressure of liquid and fluid N_2. *Phys. Chem. Liquids*, **16**, 189 (1987).
[16] C. Hoheisel. Pair and singlet translational and rotational diffusion in liquid model N_2. *Mol. Phys.*, **62**, 239 (1987).
[17] J. Vrabec, J. Stoll, H. Hasse. A set of molecular models for symmetric quadrupolar fluids. *J. Phys. Chem. B*, **105**, 12126 (2001).
[18] J. Vrabec, G.K. Kedia, H. Hasse. Prediction of Joule–Thomson inversion curves for pure fluids and one mixture by molecular simulation. *Cryogenics*, **45**, 253 (2005).
[19] B.J. Alder, D.M. Gass, T.E. Wainwright. Studies in molecular dynamics VIII. The transport coefficients of hard-sphere fluid. *J. Chem. Phys.*, **53**, 3813 (1970).
[20] C.G. Gray, K.E. Gubbins. *Theory of Molecular Fluids, Vol. 1: Fundamentals*, p. 83, Clarendon Press, Oxford (1984).
[21] A.F.M. Baron. *The Dynamic Liquid State*, pp. 23–24, Longman, London (1974).
[22] K.E. Gubbins. *Statistical Mechanics vol. 1*, K. Singer (Ed.), pp. 194–253, The Chemical Society Burlington House, London (1972).
[23] W.A. Steele. *Transport Phenomena in Fluids*, H.J.M. Hanley (Ed.), pp. 209–312, Marcel Dekker, New York and London (1969).
[24] D.J. Evans, W.B. Streett. Transport properties of homonuclear diatomics II. Dense fluids. *Mol. Phys.*, **36**, 161 (1978).
[25] R. Lustig. Angle-average for the powers of the distance between two separated vectors. *Mol. Phys.*, **65**, 175 (1988).
[26] J.M. Haile. *Molecular Dynamics Simulation*, pp. 160–163, John Wiley & Sons, New York (1997).
[27] H.C. Andersen. Molecular dynamics simulation of constant pressure and/or temperature. *J. Chem. Phys.*, **72**, 2384 (1980).
[28] D. Fincham, N. Quirke, D.J. Tildesley. Computer simulation of molecular liquid mixtures. I A diatomic Lennard–Jones model mixture for CO_2/C_2H_6. *J. Chem. Phys.*, **84**, 4535 (1986).
[29] E.W. Lemmon, M.O. McLinden, M.L. Huber. Standard reference Database 23. *REFPROP* (NIST, Version 7.0), (2002).
[30] W.M. Haynes. Mesurement of the viscosity of compressed and gaseous and liquid fluorine. *Physica*, **76**, 1 (1974).
[31] D. Levesque, L. Verlet, J. Kürkijarvi. Computer experiment on classical fluids IV. Transport properties and time-correlation functions of the Lennard–Jones liquid near its triple point. *Phys. Rev. A*, **7**, 1690 (1973).
[32] M. Shoen, C. Hoheisel. The shear viscosity of the Lennard–Jones fluid. *Mol. Phys.*, **56**, 653 (1985).
[33] F. Case, A. Chaka, D.G. Friend, D. Frurip, J. Golab, J. Russel, J. Moore, R.D. Mountain, J. Olson, M. Schiller, J. Store. The first industrial fluid properties simulation challenge. *Fluid Phase Equilibria*, **217**, 1 (2004).
[34] S. Chapman, T.G. Cowling. *The Mathematical Theory of Non-uniform Gases*, Cambridge University Press, Cambridge (1970).
[35] NIST Chemistry WebBook, http://webbook.nist.gov/chemistry.